The microstructure and phase transformations in Duplex 316L submerged arc weld metals

R. A. FARRAR
Department of Mechanical Engineering, University of Southampton, Southampton, Hampshire, UK

R. G. THOMAS
CEGB, Generation Development and Construction Division, Barnwood, Gloucester, UK

The nature and kinetics of the δ-ferrite transformation in a series of duplex submerged arc 316L weld metals has been studied under creep conditions at 600° C and an applied stress of 200 MN m^{-2}. The δ-ferrite was found to transform first to $M_{23}C_6$ carbides, these occurring at either the δ/γ interface or within the δ-ferrite laths depending upon the presence of suitable nucleation sites. The remaining δ-ferrite then transforms to the intermetallic σ-phase. The kinetics of the intermetallic phase formation varied between the different welds, and STEM/EDAX analysis indicated that the kinetics were dependent on the localized segregations of chromium, nickel and molybdenum in the δ-ferrite laths. A transformation model has been developed which indicates that chromium diffusion within the γ matrix is the controlling mechanism.

1. Introduction

The designs of current and future nuclear reactors use AISI type 316 for numerous structural components. Currently, manual processes are used for fabrication by welding. However, the submerged arc (SA) process which is semi-automatic and has high deposition rates, has economic advantages for welding heavy section, >25 mm, components. Present practice for the fabrication of such welded joints requires that the as-deposited weld metal shall contain 3 to 8% δ-ferrite to prevent hot cracking during welding, and this may be achieved using a matching 316L composition of 19Cr–12Ni–3Mo.

Although the presence of δ-ferrite is essential to obtain the correct mechanical properties during welding, the inherent instability of this phase during subsequent service conditions produces a complex series of phase transformations [1] which could have serious implications for both the creep and fracture properties of the weld metal.

Recent work by Thomas *et al.* [2] concerning the creep properties at 600° C of a series of 316L submerged arc weld metals indicated that low creep ductilities could be associated with very high, 20%, δ-ferrite contents. However, there were no other systematic variations which could be attributed to the δ-ferrite morphology, or its subsequent transformation products at 600° C.

The present paper complements these studies with an investigation into the nature of the phase transformations occurring at 600° C, and considers the significance of the segregation of chromium, nickel and molybdenum in the original δ-ferrite.

2. Experimental details

Six weld metals were deposited in the form of butt welds using different commercial wires and fluxes as given elsewhere [2], typical welding conditions being 400 A, 32–36 V, and travel speed of 305 mm min^{-1}, giving a nominal heat input of 2.7 kJ mm^{-1}. The bulk analyses of these welds are given in Table I.

Rods, 3 mm diameter, for electron microscopy were machined directly from the gauge length of

TABLE I Chemical analyses of parent plate and weld metals

Sample	Element (wt %)									Schaeffler Cr Equivalent	Schaeffler Ni Equivalent	Original % δ-ferrite
	C	S	Mn	P	Si	B	Ni	Cr	Mo			
Parent Plate	0.025	0.021	1.47	0.017	0.38	–	11.2	17.0	2.42	–	–	–
Weld 316-1	0.018	0.019	0.94	0.029	0.69	0.003	11.8	18.5	1.94	21.5	12.8	10
Weld 316-2	0.032	0.014	1.24	0.026	0.75	0.002	11.2	19.9	2.25	23.3	12.8	20
Weld 316-3	0.033	0.016	0.94	0.027	0.36	0.003	12.4	18.6	2.43	21.6	13.9	6
Weld 316-4	0.040	0.019	0.65	0.028	0.66	0.003	12.4	19.3	2.40	22.7	13.9	8
Weld 316-5	0.021	0.019	1.02	0.026	0.51	0.003	12.5	18.7	2.32	21.8	13.6	6
Weld 316-6	0.026	0.019	1.48	0.030	0.57	0.004	12.0	19.5	2.27	22.6	13.5	12

the specimens used in creep rupture tests so that the present structural investigations would relate directly to the test results.

Specimens were chosen from material that had failed at a stress of $200\,\mathrm{MN\,m^{-2}}$ in 500 to 1000 h at 600°C. After suitable slicing and mechanical polishing to $100\,\mu\mathrm{m}$ thickness, the discs were electropolished at 20°C in a manner similar to that used by Keown and Thomas [3]. Considerable difficulty was experienced in polishing weld 316-1, which could only be successfully thinned when the electrolyte temperature was kept below 10°C.

Chemical microanalyses were carried out using a JEOL JXA50A electron probe microanalyser and with an EDAX detector fitted to a JEOL 100CX scanning transmission electron microscope, STEM. The Appendix gives detail of the thin foil calibration and correction procedures adopted to obtain the STEM/EDAX profiles.

3. Results
3.1. δ-ferrite phase transformation products
Optical examination [2] had shown that there were no significant microstructural differences, with the exception of weld 316-2, which contained 20% δ-ferrite. However, quite clear differences were evident in the electron microscope.

Five main types of phase transformation were found in these weld metals and these are summarized in Table II, together with an indication of the extent to which they have occurred. Clearly, weld 316-1 represents one extreme, while weld 316-6 represents the other.

3.1.1. Type 1: very fine δ-ferrite grain boundary precipitates
These are illustrated in Figs. 1 to 3. The foils had to be correctly tilted to reveal these precipitates, which generally adopted a strain field pattern at the δ/γ boundary. Often they were associated with fringe contrast effects as shown in Fig. 2. Electron diffraction was very difficult and although no conclusive evidence as to their exact nature could be obtained, it may be presumed that they are an early stage in $M_{23}C_6$ development.

3.1.2. Type 2: large grain boundary carbides
These are clearly seen in Fig. 1 where they are associated with Type 1. In other cases they appeared to nucleate at the δ/γ boundary and grow quite rapidly into the δ-ferrite lath as seen by Thomas and Keown [1]. Fig. 4 indicates that migration of the δ/γ boundary has begun to isolate these carbides, although other examples, Figs. 5 and 6, indicate that the original boundary configuration is maintained.

Electron diffraction on the larger particles indicated that they possessed the normal orientation relationship associated with $M_{23}C_6$ carbides in austenite, namely

$$\{1\,0\,0\}_\gamma \,\|\, \{1\,0\,0\}\,M_{23}C_6$$

$$\langle 1\,0\,0 \rangle_\gamma \,\|\, \langle 1\,0\,0 \rangle\,M_{23}C_6$$

based on a cubic unit cell with $a_0 = 1.0589\,\mathrm{nm}$.

3.1.3. Type 3: dislocation associated carbides
Unlike the previous two types, these carbides adopted a random distribution within the original δ-ferrite laths, Fig. 7, and they appeared to be associated with the dislocation network within the δ-phase.

When this type of carbide precipitation was present, Types 1 and 2 were virtually absent, suggesting that they are competitive in nature and dependent on the availability of suitable nucleation sites within the δ-phase. Also, the Type 3

TABLE II Summary of δ-ferrite transformation reactions observed

| Weld number	Original δ (%)	% transformation at 600°C		δ-ferrite transformation products					Comments
		Measured	Predicted by Equation 4	Type 1: Very fine δ-ferrite grain boundary precipitates	Type 2: Large grain boundary carbides	Type 3: Dislocation associated carbides	Type 4: Divorced carbides with new γ boundaries	Type 5: σ-phase formation	
316-1	10	53	51	√√	√√	√	√	√	Many δ-ferrite laths decorated with grain boundary carbides
316-2	20	58	66	√	√	?	?	√√	
316-3	6	31	54	–	√	√√	√	√	δ-ferrite still clearly visible
316-4	8	67	64	–	√	√√	√√	√√	δ-ferrite still clearly visible
316-5	6	26	50	–	√	√√√	√√	√	
316-6	12	94	66	–	√	–	√√√	√√√	
Typical form of transformation product									

Key:
– Not observed
? Doubtful
√→√√→√√→√√√
Increased frequency.
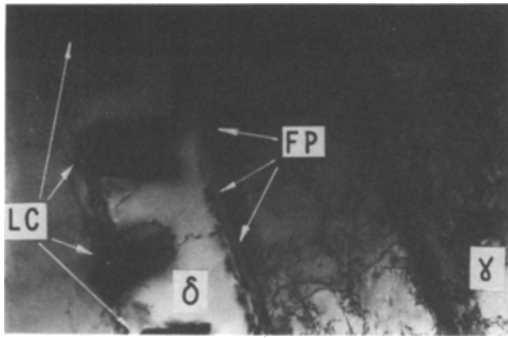
Figure 1 Grain boundary precipitates and carbides in weld 316-1 × 29 600 (FP = fine precipitate; LC = large carbides).

Figure 3 Grain boundary precipitates in weld 316-1 × 118 400.

transformation was dominant in the 316-3 and 316-5 weld metals, which had the lowest δ-ferrite contents and slowest transformation kinetics, Table II. It is of interest to note that no matrix precipitation of carbides was observed in the austenite.

3.1.4. Type 4: divorced carbides with new austenite boundaries

In the majority of the weld examined, and in particular in welds 316-4 and 316-6 which had transformed 67 and 94%, respectively, there was clear evidence of the austenite matrix growing into the original δ-ferrite lath. Fig. 8 clearly reveals that the $M_{23}C_6$ carbides decorate the location of the original δ/γ boundary, but have become divorced from the boundaries early in the transformation period as the austenite matrix grew into the δ-phase. In this particular case the remaining δ was sufficiently enriched in chromium and depleted in nickel for it to transform to σ-phase. Fig. 9 illustrates an earlier stage of this transformation in weld 316-1. The δ-ferrite has not yet transformed and the carbides are linked to the δ/γ boundary.
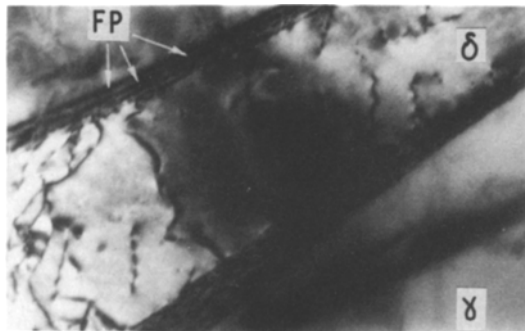
3.1.5. Type 5: intermetallic phase formation

As in the Type 4 reaction, there was clear evidence in several of the weld metals of the replacement of the original δ-ferrite by intermetallic phases, Fig. 10. Detailed examination using electron diffraction, revealed that the majority of these intermetallic transformations involved the σ-phase. Although the σ/γ orientation relationship was variable, a frequently noted relationship was

$$(1\,1\,1)_\gamma \parallel (0\,0\,1)_\sigma$$

$$\langle 0\,1\,1 \rangle_\gamma \parallel \langle 1\,4\,0 \rangle_\sigma$$

with lattice parameters $a_0 = 0.881 \pm 0.002$ nm and $c_0 = 0.455 \pm 0.002$ nm which are similar to those reported by Weiss and Stickler [4]. Although some evidence was obtained for the χ-phase, no definitive electron diffraction patterns could be obtained. However, it had been detected earlier by X-ray diffraction measurements on the bulk samples [2].

As Keown and Thomas [3] had reported the presence of carbides at the austenite grain boundaries, these boundaries were studied in the present weld metals. Apart from a few isolated car-

Figure 2 Grain boundary precipitates associated with fringe contrast at the δ/γ boundary in weld 316-1 × 92 500.

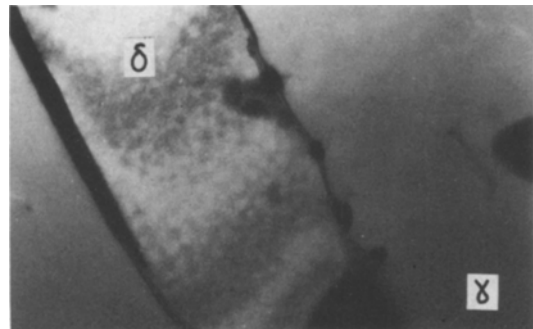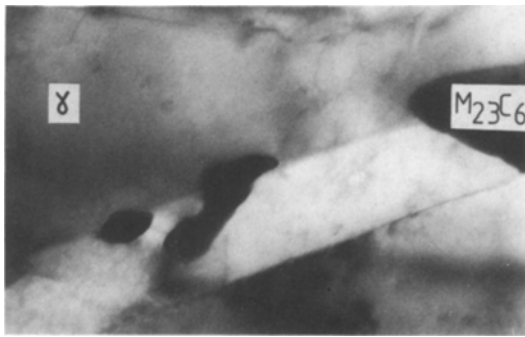Figure 4 Early development of large grain boundary carbides in weld 316-1 × 59 200.

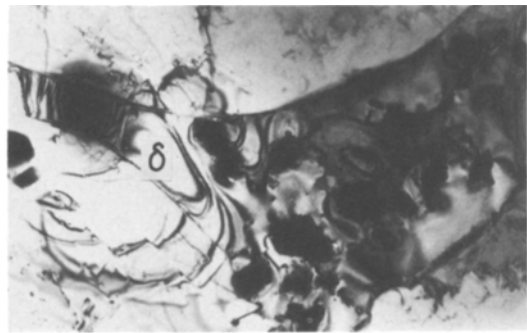*Figure 5* Very large $M_{23}C_6$ carbides in weld 316-1 × 59 200.

Figure 7 Dislocation associated carbide precipitation in weld 316-5 × 14 800.

bides, Fig. 11, no significant development of carbides was observed at the γ/γ boundaries.

3.2. Concentration profiles

The segregation of chromium, nickel and molybdenum was determined using both electron probe microanalysis and STEM/EDAX microanalysis on suitable samples of the weld metals. For electron probe microanalysis, bulk samples polished to 0.25 μm diamond finish were used, whereas STEM/EDAX analyses were performed directly on the thin foils.

The results of electron probe analysis for weld 316-5, after creep testing for 470 h at 600° C, indicated segregation of chromium and molybdenum to the δ-ferrite phase, Fig. 12, with a systematic depletion in nickel. Although the resolution of the technique is only 2 to 3 μm, clear concentration profiles were obtained from the 1 to 2 μm thick δ-ferrite laths. These results suggested that the chromium and nickel profiles in the austenite matrix are relatively smooth.

Measurements on other welds revealed similar compositional profiles.

As a check on the stability of these segregation profiles, weld 316-5 was heat treated for a further 500 h at 775° C and remeasured on the electron probe. Only minor differences in the profiles were detected, indicating the very slow diffusion rates once the intermetallic phases have been formed.

The results of the STEM/EDAX microanalysis on thin foils indicated similar results to the bulk microprobe analysis but with a higher resolution. Fig. 13 illustrates a typical profile obtained, see Appendix for correction procedures. In all cases, segregation of chromium and molybdenum to the original ferrite, together with a systematic depletion of nickel, was observed, although the magnitude was different between the samples. Of particular interest is the segregation of molybdenum to the γ/δ and possibly γ/σ boundaries, suggesting that the grain boundary carbides may be incorporating molybdenum into the structure as suggested by Weiss and Stickler [4] and Keown and Thomas [3].

Examination at higher magnification allowed detailed microanalysis to be made in places where the austenite matrix had migrated into the original δ-phase thus isolating the original γ/δ boundary carbides. An example of this is shown in Fig. 14.
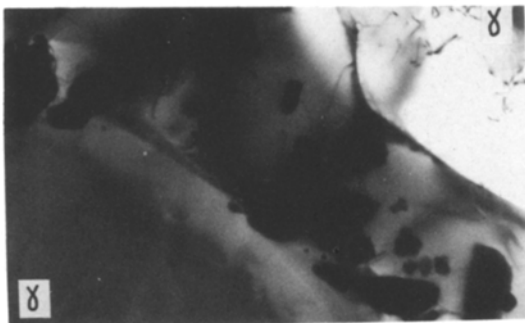

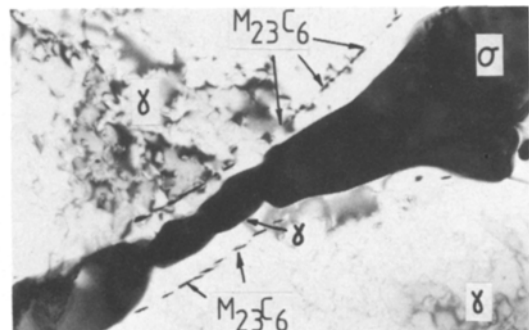*Figure 6* Large $M_{23}C_6$ carbides and dislocation associated carbide precipitation in weld 316-2 × 24 420.

Figure 8 Divorced $M_{23}C_6$ carbides with new γ/σ boundaries in weld 316-6 × 14 800.
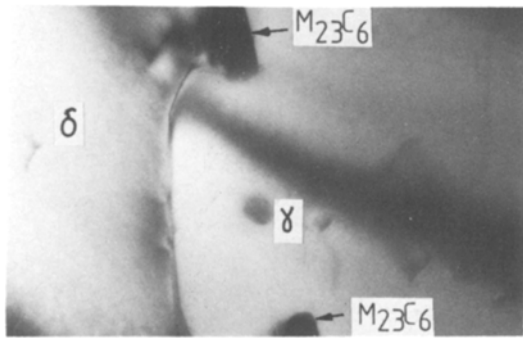
3465

Figure 9 $M_{23}C_6$ carbides at the δ/γ boundary. Evidence of the early stages of boundary movement in weld 316-1 ×92 500.
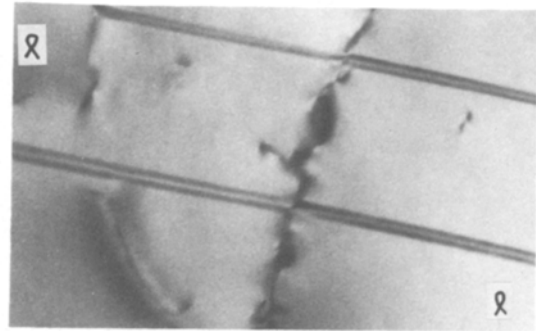

Figure 11 Austenite grain boundaries containing a few $M_{23}C_6$ carbides. Strain bands are visible in the austenite in weld 316-4 × 148 000.

There appears to be a relatively smooth change in the chromium and nickel profiles across the matrix and the new γ/δ or γ/σ boundary.

The segregation of molybdenum is obviously more complex with an enrichment occurring in the initial $M_{23}C_6$ carbides which are decorating the original austenite boundary. The austenite boundary in both these cases has moved ~0.5 to 0.8 μm from its original position.

3.3. Phase diagram relating to 316 materials

Although the Schaeffler diagram may be used to predict the amount of metastable δ-ferrite which will be formed in welding, subsequent heat treatment during creep testing will allow the metastable phases to move towards the equilibrium conditions. The phase diagram for the ternary Fe–Cr–Ni system [5] is shown in Fig. 15 with the phase boundaries in the iron rich corner; although the creep testing was conducted at 600° C it is felt

that only small shifts in these boundaries will occur between 650 and 600° C.

Using the as-welded bulk analyses* it can be seen that all the welds lie within the $\sigma + \gamma$ phase field at 650° C. However, using the values obtained from the STEM/EDAX analyses on the transforming δ-ferrite laths, it is clear that whereas welds 1, 2 and 4 still lie within the $\sigma + \gamma$ phase field, the ferrite in welds 3 and 5 lies on the boundary of the $\sigma + \gamma$ and the $\sigma + \gamma + \delta$ fields; and that in the case of weld 6 the values are closest to the σ field.

4. Discussion
4.1. Segregation profiles in 19/12/3 materials

It has been suggested by Lippold and Savage [6] that at normal cooling rates, 316 stainless steel weld metals solidify according to the Case 3 solidification conditions. In Case 3 solidification, there is no diffusion in the solid and no mechan-

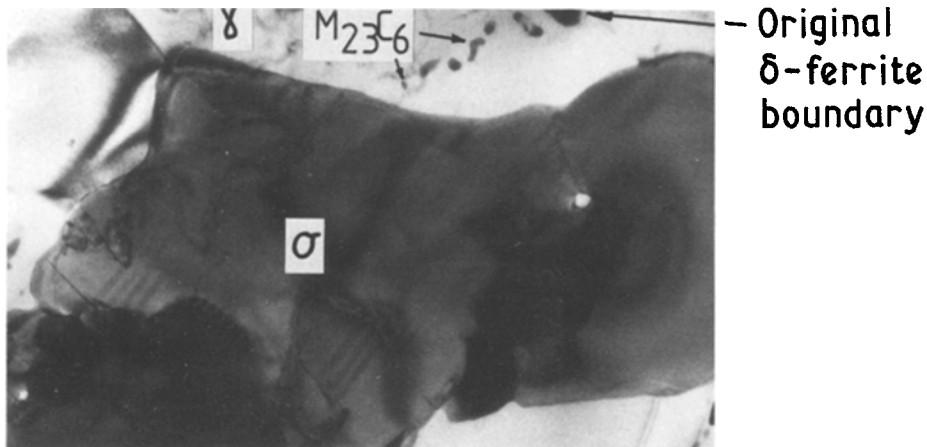– Original δ-ferrite boundary

Figure 10 Striated σ-phase. $M_{23}C_6$ carbides at the original δ/γ boundary in weld 316-3 × 40 000.

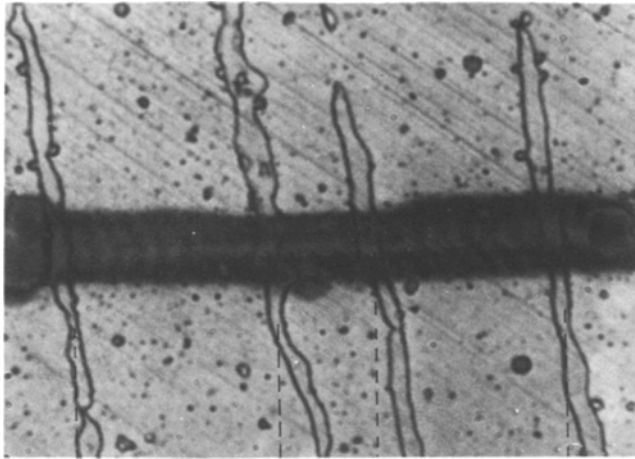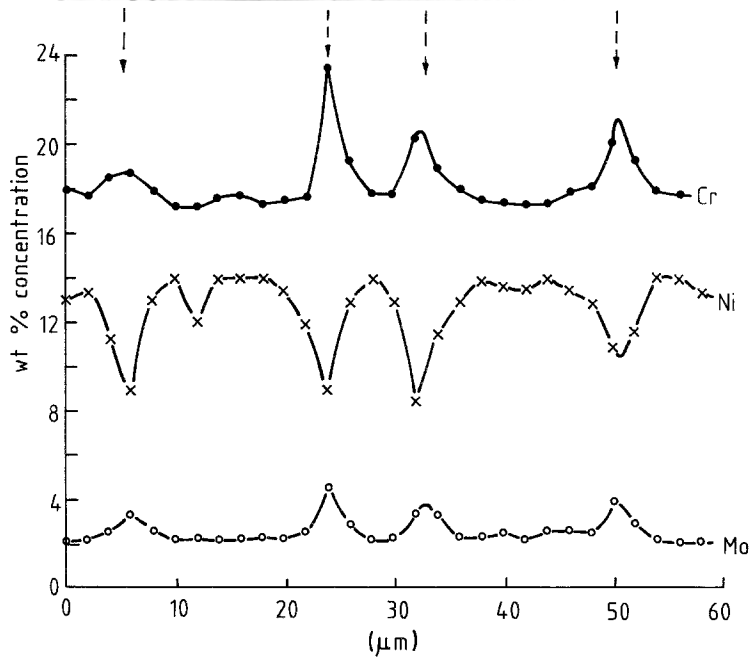*These analyses have been based on the Schaeffler chromium and nickel equivalent compositions, Table I.

ical mixing in the liquid. Concentration changes in the liquid occur only by diffusion.

Each advancing cell or cellular dendrite has an initial transient region at its core, which is enriched in ferrite stabilizing elements such as chromium and molybdenum, and a final transient region enriched in the austenite stabilizing elements such as nickel, Fig. 16. Between these two transient regions, there is a region of steady state growth.

On subsequent cooling through the $\delta + \gamma$ region, the cooling rates in welding would be too rapid to alloy the γ to form by a simple diffusion mechanism, and a "massive" transformation would have to occur as suggested by Massalski *et al.* [7]. However, the ferrite formed at the dendrite core remains stable at room temperature as it lies

within the single phase region due to enrichment of chromium and molybdenum. It is this δ-ferrite which will transform at service temperatures to a mixture of carbides and intermetallic phases.

It is apparent from the concentration profiles measured using conventional EPMA and STEM/ EDAX and illustrated in Figs. 12 and 13, that the model of Lippold and Savage [6] may be applied to the present results. These profiles reveal the enrichment of chromium and molybdenum in the initial transient region at the dendrite cores followed by the relatively constant values of chromium, nickel and molybdenum in the steady state region between the dendrite cores. There was, however, no evidence for the changes in the chromium and nickel levels which are predicted by the model for the final transient region. Lippold
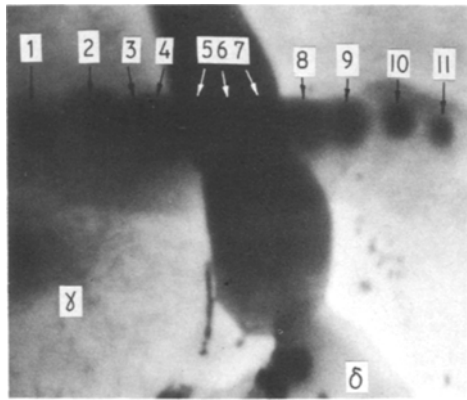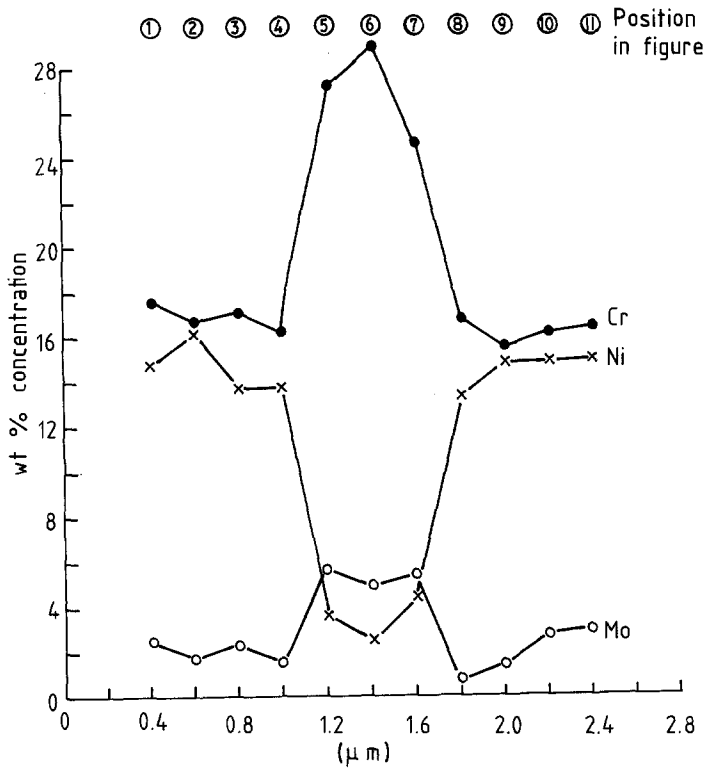
3467

and Savage were also unable to detect this final transient region in their studies on a 19Cr–10Ni 304L stainless steel weld metal, although Lyman [8] has reported a 1% rise in the nickel concentration using STEM/EDAX microanalysis on a similar type of weld metal.

A detailed examination using the STEM/EDAX technique failed to reveal this final transient region in the current weld metals; in all cases the chromium and nickel profiles varied quite smoothly between the delta ferrite laths. Thus, it may be concluded that this effect is either absent or is too small to be measured by either electron probe or STEM/EDAX microanalysis.

After a further heat treatment of weld 316-5 at 775°C for 500 h, in which the δ-ferrite completely transformed to σ-phase, microprobe analysis indicated that the concentration profiles were relatively unchanged, confirming the stability of the σ-phase at this temperature.

Considering the diffusion of chromium in the austenite away from the transforming δ lath as the controlling mechanism, the mean shift, $\bar{x}$, in the profile can be calculated from the general expression, $\bar{x} \propto (Dt)^{1/2}$. Using $D = 4.6 \times 10^{-18}\,\mathrm{m^2\,sec^{-1}}$ at 775°C, Smith [9], and $t = 500\,\mathrm{h}$; $\bar{x} = 2.5\,\mu\mathrm{m}$. This shift would be barely detectable by electron probe analysis, and further studies using STEM/EDAX are currently in progress to study the decay of
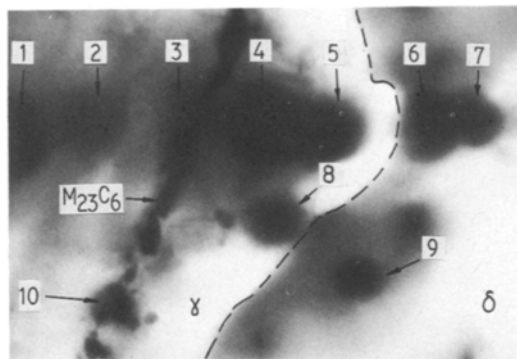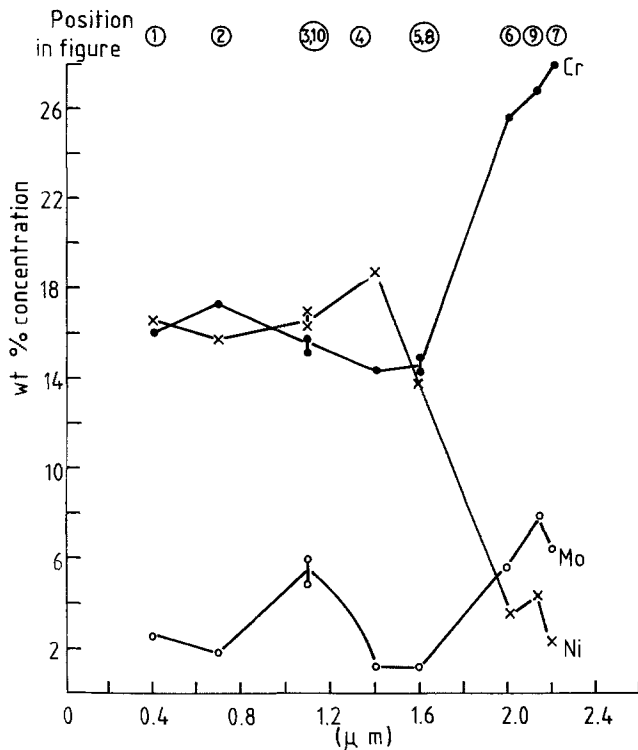
Figure 14 Compositional profile across isolated $M_{23}C_6/\gamma$ boundary in weld 316-6 using STEM/EDAX. Foil thickness 210 nm. (Note positions 8, 9, 10 are plotted at the correct distance from the γ boundary).

these profiles, when as-welded samples are systematically aged at 600 to 700°C.

The δ-ferrite which remains stable at room temperature after welding is therefore highly enriched in chromium and molybdenum, while the austenite will be supersaturated in carbon. It is the diffusivity of the carbon and chromium atoms which then controls the subsequent phase transformations at the service temperatures.

4.2. Transformation model for 19/12/3 materials

Previous studies by Thomas and Keown [1] indicated that there is a sequential mechanism for these transformations, and this is supported by the present work.

Initially, the δ-ferrite will break down via a eutectoid-type reaction at the γ/δ boundary to a mixture of $M_{23}C_6$ carbides and austenite, Figs. 1 and 4. The nucleation of these carbides and their growth will depend upon the availability of chromium from the delta phase, the rapid diffusion of carbon from the austenite and the crystallographic correspondence of the cubic carbide cell with the surrounding γ matrix [10].

The localized chromium denudation of the ferrite by the carbides allows the austenite phase to grow between the cellular carbides, but as the carbon from the austenite is rapidly consumed, the growth of the $M_{23}C_6$ carbides slows down allowing the austenite to continue to grow controlled by the chromium diffusion from the δ-phase. The boundary will eventually break away from the carbide decorated interface as illustrated in Fig. 9.
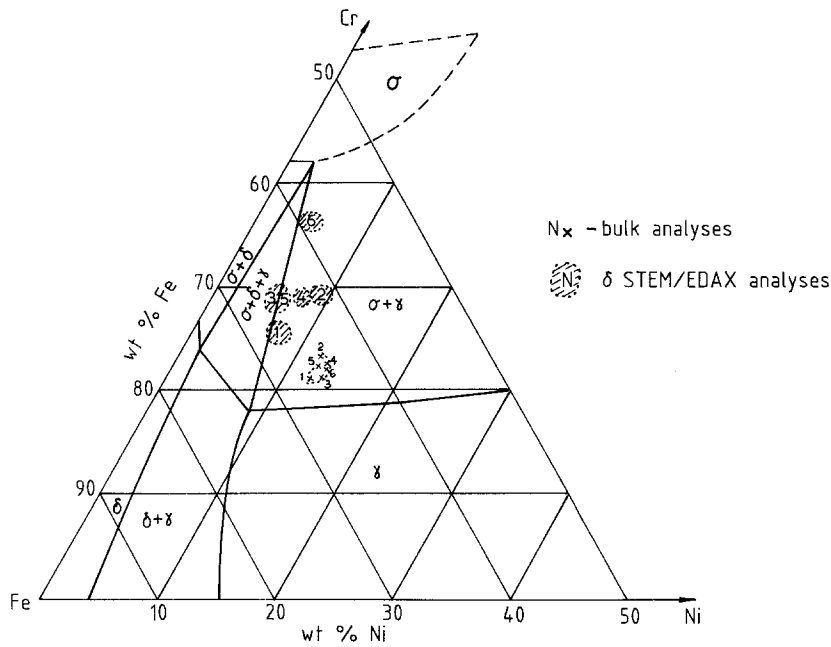
Figure 15 Fe-rich portion of the Fe–Cr–Ni phase diagram at 650° C (after [5]).

Weiss and Stickler [4] have suggested that molybdenum may assist in the nucleation and growth of $M_{23}C_6$ carbides and certainly it plays a significant part in their subsequent conversion to the M_6C carbides. Some limited evidence for the presence of M_6C was obtained, and the molybdenum profiles obtained by STEM/EDAX analysis, Fig. 14, indicate that molybdenum was present in the grain boundary carbides which were decorating the original δ/γ boundaries. Further studies are being undertaken to clarify the exact role of molybdenum in this phase transformation.

The formation of $M_{23}C_6$ carbides within the δ-ferrite phase is more difficult to explain since it requires the diffusion of carbon from the austenite to the nucleation sites. These sites are apparently dislocations which have developed on cooling and may have been introduced by the transformation stresses set up when the matrix ferrite transformed to austenite.

Certainly in welds 316-3 and 316-5, the nucleation of carbides was frequently observed occurring on dislocation sites within the δ-ferrite and it was in these weld metals that the transformation kinetics were slow due to the lower enrichment of chromium in the ferrite.

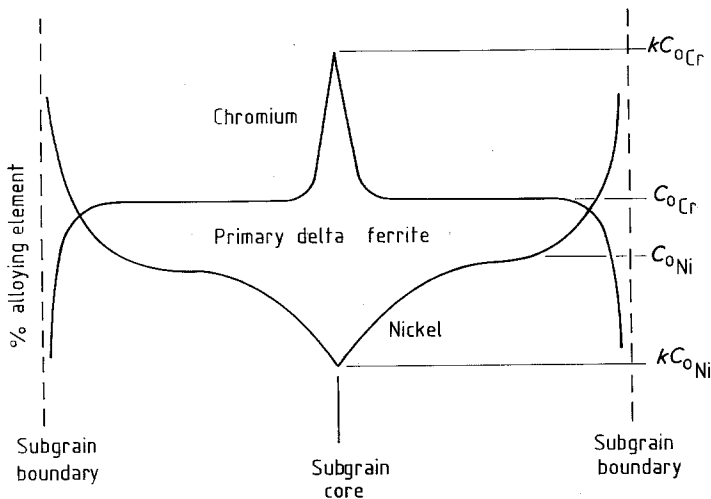As the amount of the carbon available is limited, the formation of the Type 3 carbides must

Figure 16 Lippold and Savage model for concentration profiles in primary δ-ferrite (after [6]).

be competitive with Types 1 and 2 and their formation will cease when the carbon is exhausted.

Lewis [11] and Beckett [10] have suggested that carbides can act as nuclei for the growth of the σ-phase, especially in stressed conditions. The growing carbides, due to their volume mismatch with the austenite, punch out dislocations into the surrounding matrix, and these dislocations form ideal sites for σ nucleation. However, the higher energy sites such as the triple points, and at δ/γ boundaries favour the direct nucleation of the σ- and χ-phases [12]. Other nucleation sites are stacking faults and dislocation tangles. After nucleation, this reaction eventually proceeds to the complete replacement of the δ-ferrite by σ as illustrated by Fig. 8.

Thomas and Keown [1] suggest that the σ-phase continues to grow at the expense of the $M_{23}C_6$ precipitates which are redissolved. No evidence of this was obtained in the current work after 1000 h at 600°C in which there were numerous examples of the σ-phase coexisting with original $M_{23}C_6$ carbides at the divorced original γ/δ boundary, Fig. 8, but it might occur at higher temperatures or longer transformation times.

Numerous stacking faults were observed within the σ-phase, Fig. 10, and it is suggested that these faults are due to the coincidence of the (1 1 1) planes of the austenite which have an ABCABC... packing, with the (0 0 1) planes of σ, which have an ABAB... packing. The segregation of molybdenum to the original γ/δ boundary may also be important as suggested by Wegrzyn and Klimpel [13], who found that molybdenum accelerated the formation of the σ-phase.

Although the inherent inhomogeneity of the weld metals will allow different reactions to occur, a typical reaction sequence at 600°C may be postulated as follows:

1. Rapid diffusion of carbon from the austenite to the δ/γ boundaries.

2. Incorporation of chromium and molybdenum from the ferrite to produce $M_{23}C_6$ carbides.

3. Localized denudation of chromium and carbon from the δ/γ boundary allows the transformation of δ → γ.

4. Cellular γ + $M_{23}C_6$ precipitates grow until the carbide growth ceases due to exhaustion of carbon.

5. The austenite advances into the δ-ferrite lath, controlled by chromium diffusion, within the austenite thus divorcing the $M_{23}C_6$ carbides.

6. Depending upon the precise nature of the nuclei present and the levels of chromium and molybdenum segregation, intermetallic phases such as σ nucleate and grow to consume the remaining δ.

4.3. Diffusion control of phase transformation reactions

Adopting the diffusion analysis employed in the calculation of the average concentration of gas remaining in a metal during degassing experiments, Shewmon [14] was able to show that the average carbon content, $\bar{C}$, of the austenite matrix at any time, t, was given by the simplified expression:

$$\bar{C}(t) = \frac{8C_0}{\pi^2} \exp\left(-\frac{\pi^2 D_c^\gamma t}{\lambda_\gamma^2}\right) \qquad (1)$$

where C_0 was the initial carbon content, D_c^γ was the diffusivity of carbon in γ-iron and λ_γ was the austenite mean free path. If we assume in a duplex steel that the value of λ_γ represents the average δ lath spacing, say 0.02 mm, that the initial carbon concentration is 0.05% and that the limiting value of $\bar{C}$ is solubility level for $M_{23}C_6$ at 600°C, say 0.005 wt %, the time t_i at which the δ/γ interface isolates the carbides in the matrix may be calculated as:

$$t_i = \frac{\lambda_\gamma^2}{\pi^2 D_c^\gamma} \ln\left(\frac{8C_0}{\pi^2 \bar{C}}\right) \qquad (2)$$

which gives a value of 0.38 h for $D_c^\gamma = 6.55 \times 10^{-14}\,\text{m}^2\,\text{sec}^{-1}$. Thus Equation 2 predicts rapid diffusion of carbon to the nucleating and growing carbides in a very short time compared to the 500 to 1000 h used during the creep testing of the sample.

If we assume that all the chromium for the $M_{23}C_6$ comes from the δ it is obvious that the concentration profiles will change very little in the bulk of the ferrite laths during this time and that the transformation must now be controlled by the diffusivity of chromium away from the lath into the advancing austenite interface bowing out from the isolated carbides.

The situation can be modelled as shown in Fig. 17a which represents the initial situation before the precipitation of the carbides with a very steep profile between the δ-ferrite and the austenite matrix. If we allow the interface to move from x_0, the position at which the $M_{23}C_6$ carbides precipitate, to x_t, then the rate of interface movement will be controlled by the diffusivity of chromium
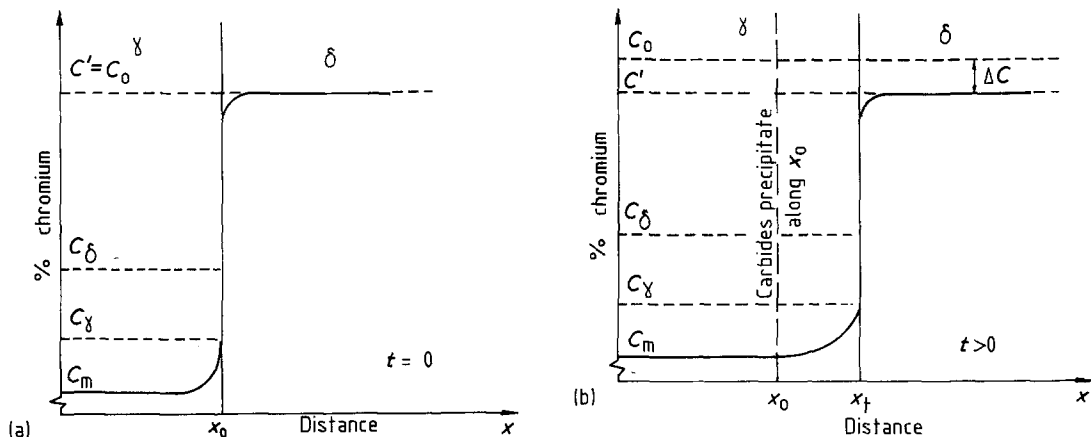
Figure 17 Chromium profiles: (a) as-welded condition and (b) after creep testing at 600° C.

in the austenite. Using a simple mass balance approach we have:

$$(D_{Cr}^{\gamma} t)^{1/2}(C_{\gamma} - C_{m}) = (x_{t} - x_{0})\Delta C \qquad (3)$$

where C_{γ} is the concentration of chromium in the austenite at the δ/γ interface, C_{m} is the concentration of chromium the austenite remote from the δ/γ interface, and ΔC is the drop in the maximum chromium concentration in the δ-ferrite lath. These are illustrated in Fig. 17b.

From the measurements obtained on weld 316-6, $(x_{t} - x_{0}) = 0.4 \to 0.8\,\mu m$, $(C_{\gamma} - C_{m}) = 6\,wt\%$ and $D_{Cr}^{\gamma} = 1.82 \times 10^{-20}\,m^{2}\,sec^{-1}$ [9], giving a value of $\Delta C = 2.5\,wt\%$ in 1000 h of testing, which is small compared to the initial value of $(C' - C_{\delta}) = 10\,wt\%$. In the case of weld 316-3, the value of ΔC is 0.5 wt %, compared with the original value $(C' - C_{\delta})$ of 5 wt %.

It can be concluded, therefore, that there is still sufficient chromium in the δ-ferrite after testing at 600° C to form the σ-phase.

4.4. Influence of ternary Fe—Cr—Ni phase diagram

Earlier work by Thomas and Yapp [15] on manual metal arc deposits of similar composition to the present weld metals, indicated the rate of transformation of the δ-ferrite could be described by Equation 4:

$$\ln\left[-\ln(1-x)\right] = 19.32 - \frac{19860}{T} + \frac{\ln t}{2} \qquad (4)$$

where x is the fraction transformed after t hours at temperature T K.

Applying Equation 4 to the results obtained

with the present welds, indicated significant deviations from the expected values, Table II. For example, weld metals 316-3 and 5 have transformed more slowly, whilst weld 316-6 has transformed more rapidly than Equation 4 would predict.

From the bulk analyses of the weld metals, Table I, it was expected that the δ-ferrite would transform during creep testing to a mixture of $M_{23}C_{6}$ and σ-phases. In Fig. 15, the bulk analyses are plotted on the isothermal section of the Fe—Cr—Ni phase diagaram at 650° C, and they all clearly lie within the $\sigma + \gamma$ phase field.

If, however, the segregation analyses values are plotted, different groupings emerge. Welds 316-1, 2 and 4 lie within the $\sigma + \gamma$ field, welds 316-3 and 5 lie within the $\sigma + \delta + \gamma$ field and weld 316-6 lies closest to the σ-phase field.

It is suggested that these variations in the localized segregation of chromium and nickel in the δ-ferrite laths effectively control the transformation kinetics due to the different final equilibrium transformation products predicted by the phase diagram. If the initial segregation values could be controlled by changes in consumables and/or cooling rates after welding, then it may be possible to limit σ formation at service temperatures.

In order to specify the appropriate compositions and welding parameters it will be necessary to establish the relationships which govern the initial chromium and molybdenum segregation during the initial transient region. If these can be kept low, consistent with the formation of 5 to 10% δ-ferrite, then the weld metal should have a much lower propensity to the formation of inter-

metallic phases after the $M_{23}C_6$ carbides have been precipitated at the δ/γ boundaries.

5. Conclusions

1. After creep tesing at $600°C$, the original δ-ferrite in the weld metals transforms to varying extents, to mixtures of $M_{23}C_6$ carbide and σ-phase.

2. The δ-ferrite transformation to $M_{23}C_6$ can occur at either the original δ/γ boundaries or within the δ-ferrite, depending upon the availability of suitable nucleation sites. After the exhaustion of carbon within the γ matrix, the austenite boundary grows into the δ-ferrite and the $M_{23}C_6$ carbides are divorced from the migrating boundary.

3. The σ-phase is nucleated within the δ-ferrite laths, and it occurs after the precipitation of the $M_{23}C_6$ carbides. The kinetics of formation of the σ-phase appears to depend on the enrichment of chromium and molybdenum within the laths, and the proximity of the local δ-ferrite composition to the ternary equilibrium phase boundaries at $600°C$.

4. The concentration profiles of chromium, molybdenum and nickel do not vary in the γ matrix, but there is an enrichment of chromium and molybdenum and a depletion of nickel within the δ-ferrite. These profiles do not alter significantly with extended heat treatment at $775°C$, indicating the stability of the transformation products formed.

5. Evidence of molybdenum segregation to the δ/γ boundaries suggested that it was being incorporated into the $M_{23}C_6$ carbides.

6. A transformation model for δ-ferrite in 19/12/3 materials has been developed which indicates that chromium diffusion within the γ-phase is the controlling mechanism.

Acknowledgements

Appendix: Calibration of the STEM/EDAX method — k factors

The original work of Cliff and Lorimer [16] suggested that if the "thin foil condition" was used then the primary X-rays generated within the foil had a low probability of interacting with the sample, i.e. they were neither absorbed nor caused fluorescence. In this case, the simple expression (Equation A1) can be used:

$$\frac{I_1}{I_2} = k \frac{C_1}{C_2} \qquad (A1)$$

where I_1 and I_2 are the measured characteristic X-ray intensities, C_1 and C_2 are the weight fractions of the two elements in question and k is a factor which depends upon the instrument conditions used.

In a review of the correction procedures for thin foil analysis, Goldstein et al. [17] have quoted the following values of k, normalized to Fe = 1.0 for the elements of interest to this study. These compare well with the original values quoted by Cliff and Lorimer [16].

	Goldstein values	Cliff and Lorimer values
$CrK\alpha$	0.87	0.85
$MnK\alpha$	0.98	0.96
$FeK\alpha$	1.00	1.0
$NiK\alpha$	1.08	1.15
$MoL\alpha$	--	3.0

During the calibration of the JEOL 1000X + EDAX detector employed in the present work, it was found that using a standard 316 steel which had been analysed by bulk wet analysis, electron probe with wavelength dispersion, and electron probe with EDAX facilities and found to contain 17% Cr, 11% Ni, 2.4% Mo and 1.5% Mn, that the k factors were not correct and that the following values were needed to obtain the correct results from the background stripped intensity ratios.

$CrK\alpha$	0.75
$MnK\alpha$	0.95
$FeK\alpha$	1.00
$NiK\alpha$	1.50
$MoL\alpha$	3.5

indicating that even in the thin foil condition there was a significant fluorescence effect of $FeK\alpha$ on chromium which systematically caused absorption of the $NiK\alpha$ radiation. The presence of the fluorescence effect has recently been discussed by Nockolds et al. [18] who found with an Fe—10.5 wt% Cr alloy that a 10% correction needed to be made to the computed k factors owing to fluorescence occurring.

References

1. R. G. THOMAS and S. R. KEOWN, "Mechanical Behaviour and Nuclear Applications of Stainless Steel at Elevated Temperatures" Varese Conference, May 1981 (Metals Society, London, 1982) Book 280.
2. R. G. THOMAS, R. D. NICHOLSON and R. A. FARRAR, submitted to *Met. Technol.*
3. S. R. KEOWN and R. G. THOMAS, *Met. Sci.* **15** (1981) 386.
4. B. WEISS and R. STICKLER, *Met. Trans.* **3** (1972) 851.
5. V. G. RIVLIN and G. V. RAYNOR, *Int. Met. Rev.* **248** (1980) 21.
6. J. C. LIPPOLD and W. F. SAVAGE, *Weld. J. Res. Suppl.* **58** (1979) 362s.
7. T. B. MASSALSKI, A. J. PARKINS and J. JAKL-OVSKY, *Met. Trans.* **6A** (1975) 1405.
8. C. E. LYMAN, *Weld. J. Res. Suppl.* **58** (1979) 189s.
9. A. F. SMITH, *Met. Sci.* **10** (1975) 375.
10. F. R. BECKETT, *J. Iron Steel Inst.* **207** (1969) 632.
11. M. LEWIS, *Acta Metall.* **14** (1966) 1421.
12. J. K. L. LAI and J. R. HAIGH, *Weld. J. Res. Suppl.* **58** (1979) 1s.
13. J. WEGRZYN and A. KLIMPEL, *ibid.* **60** (1981) 146s.
14. P. G. SHEWMON, "Diffusion in Solid" (McGraw Hill, New York, 1963).
15. R. G. THOMAS and D. YAPP, *Weld. J. Res. Suppl.* **57** (1978) 361s.
16. G. CLIFF and G. W. LORIMER, *J. Microsc.* **103** (1975) 203.
17. J. I. GOLDSTEIN, J. L. COSTLEY, G. W. LORIMER and S. J. B. REED, "Scanning Electron Microscopy", Vol. 1, edited by O. Johan (ITRI, Chicago, Illinois, 1977) p. 315.
18. C. NOCKOLDS, M. J. NASIR, G. CLIFF and G. W. LORIMER, "Institute of Physics Conference Series" No. 52 (1980) Chap. 9, p. 417.